

Numerical Simulations of The Net Current in the Gulf of Thailand Under Different Monsoon Regimes

**Anond Snidvongs¹
Pramot Sojisuporn²**

¹Marine Science Department, Chulalongkorn University

²Harbour Department, Ministry of Communication

ABSTRACT

Net circulation in the three layers in the Gulf of Thailand 0-10 m, 10-40 m and >40 m were simulated by a hydrological model using tri-monthly average of observed temperature, salinity, depth and wind. Prevailing monsoon was an important factor controlling current speed and direction of water above the pycnocline (0-40 m). The water in the upper 10 m flew from the South China Sea during the Northeast Monsoon and opposite during the Southwest Monsoon. The water in the near surface layer in all simulations was replenished mainly by the opposite flow in the mid-depth layer and only slightly from the deep, nutrient enriched, water below 40 m. The true circulation gyre could not be seen in our simulations but different degrees of eddies and meanders were evident in almost all runs. These features could play very important roles in the distribution and dispersion of dissolved, particulate and biological species, including pollution and larvae, and deserved more in depth studies in the future.

Introduction

The net circulation is an important factor that governs the distribution, dispersion and residence time of dissolved and suspended materials, biotic as well as abiotic forms, in the water. It is a basic information frequently required to explain the results of other chemical and biological studies of seawater.

The net circulation pattern of a large area, such as the Gulf of Thailand and Eastern Peninsular Malaysia is difficult and very costly to obtain. Direct observation by mean of deployment of a large number of current meters, each covers the time period at least 1 tidal cycle (i.e. 15 days), is definitely impossible during this SEAFDEC Collaborative Research Program. Existing current observation data available from several data centers worldwide are however few and the stations were too far apart to able to interpolate the result to get a reasonable picture of current field.

The lack of current data and the difficulties in obtaining them for large study areas are not uncommon problems among marine and coastal studies. Hydrologists and oceanographers, therefore, have developed a well established approach of numerical modeling to get around the problems. By using concepts and theories in classical physics, forcing functions for water movement and circulation can be described and interrelated by mathematical equations. The suites of equations are subsequently solved for velocity and other variables using numerical techniques.

In this report, we will attempt to simulate the net circulation, that is free from tidal effects, for the Gulf of Thailand. The coastal shelf off the Peninsular Malaysia, however, is too open to the South China Sea and the condition for the model that the open boundary must be horizontally homogeneous may not be true for this case, thus the area was excluded.

The model used in this study had been successfully implemented for the upper Gulf of Thailand, which is a small (100 km x 100 km) bay situated at the northernmost part of the Gulf (Sojisuporn 1995). The model relates the water movement in three dimension with the oceanographic variables easily and frequently measured, and therefore can cover extensive area within a short sampling period, i.e. temperature, salinity and meteorological data. However the reader must always aware that

the simulation done here is only a simplification of the natural system, where there are much more factors involved. Many of those may occur only in small areas and/or in short time periods. These small scale temporal and spatial variations are usually missed by the sampling programs especially when spatial data is not collected simultaneously. For the purpose of obtaining the general picture of the current field of a large area, there are usually irrelevant in term of time and space scales.

Numerical Model

The governing equations are the momentum equations, the continuity equation, and the conservation of heat and salt. The momentum equations are used to calculate horizontal velocity components. The equations retain temporal changes, field accelerations, the Coriolis effects, pressure gradient terms, and horizontal and vertical eddy viscosities. Using conventional notations in the left-hand Cartesian coordinate, the momentum equations for horizontal velocities are written as

$$\frac{fu}{ft} + u \frac{fu}{fx} + v \frac{fu}{fy} + w \frac{fu}{fz} - fv = -\frac{1}{\rho_0} \frac{fP}{fx} + A_h \frac{f^2 u}{fx^2} + A_h \frac{f^2 u}{fy^2} + A_v \frac{f^2 u}{fz^2} \quad (1)$$

$$\frac{fv}{ft} + u \frac{fv}{fx} + v \frac{fv}{fy} + w \frac{fv}{fz} + fu = -\frac{1}{\rho_0} \frac{fP}{fy} + A_h \frac{f^2 v}{fy^2} + A_h \frac{f^2 v}{fx^2} + A_v \frac{f^2 v}{fz^2} \quad (2)$$

where: x and y are horizontal axes

z is vertical axis

t is time

u and v are horizontal velocity components corresponding to x and y axis, respectively

f is the Coriolis parameter ($2W \sin f$, where f is latitude)

ρ_0 is density

A_h and A_v are horizontal and vertical eddy viscosity coefficients, respectively.

The pressure terms are represented by both hydrostatic and buoyancy terms, and are expressed as

$$P = \rho_0 g \xi - \rho_0 \int_0^z B dz \quad (3)$$

$$B = \frac{\rho_0 - \rho}{\rho_0} g \quad (4)$$

where: g is gravitational acceleration (980 cm s^{-2})

B is buoyancy force

ρ is referenced density

The continuity equation is used for the calculation of water surface elevation and vertical velocity component. The equation can be expressed as

$$\frac{fu}{fx} + \frac{fv}{fy} + \frac{fw}{fz} = 0 \quad (5)$$

The water surface elevation is calculated from vertical velocity at the surface:

$$\frac{f\eta}{ft} = -W_s \quad (6)$$

where: h is water surface elevation
 W_s is vertical velocity at the surface.

The conservation of heat and salt are used to calculate the changes of these two parameters due to advection and diffusion processes (Sarmiento and Bryan, 1982). The equations also include the terms that draw the calculated values to the observed ones. The equations are written as

$$\frac{\partial T}{\partial t} + u \frac{\partial T}{\partial x} + v \frac{\partial T}{\partial y} + w \frac{\partial T}{\partial z} = K_h \frac{\partial^2 T}{\partial x^2} + K_h \frac{\partial^2 T}{\partial y^2} + K_v \frac{\partial^2 T}{\partial z^2} + \gamma(T^* - T) \quad (7)$$

$$\frac{fS}{ft} + u \frac{fS}{fx} + v \frac{fS}{fy} + w \frac{fS}{fz} = K_h \frac{f^2 S}{fx^2} + K_h \frac{f^2 S}{fy^2} + K_v \frac{f^2 S}{fz^2} + \gamma(S^* - S) \quad (8)$$

where: T and S are modeled temperature and salinity, respectively
 K_h and K_v are horizontal and vertical diffusivity coefficients, respectively
 T^* and S^* are observed temperature and salinity, respectively.

The g terms in (7) and (8) are introduced by Sarmiento and Bryan (1982) to prevent the deviations of calculated T and S values from the observed ones. The value of g indicates the degree of modification of the observed values by the local advective-diffusive balance (Fujio and Imasato, 1991). For a small or zero g , the model is nearly independent or independent of the observed values, approaching the prognostic model (Yanagi and Takahashi, 1993). For a large g , the model is restricted by the observed values, approaching diagnostic model (Fujio and Imasato 1991).

Full-slip condition is employed at the lateral walls. The bottom stress is given as

$$A_v \frac{\partial u}{\partial z} = \gamma_b |u|u \quad (9)$$

where: γ_b is bottom drag coefficient
 u is horizontal velocity in the bottom layer.

The surface momentum flux from the wind is given as

$$\rho_0 A_v \frac{\partial u}{\partial z} = \rho_a C_d |W|W \quad (10)$$

where: ρ_a is air density (0.0012 g cm⁻³)
 C_d is surface drag coefficient
 W is wind velocity.

There is no flux of temperature and salinity at the lateral walls, the water surface, and the bottom. Cramped open boundary condition and sponge layers are used at the open boundary (for definition see Roed and Cooper, 1986). Tidal forcing is neglected because we want to obtain velocity field at steady state. The leap-frog scheme is used with centered difference in space and forward in time. Backward computation was inserted every 10 time steps. And semi-implicit scheme is employed for the calculation of water elevation (Backhaus, 1983).

Model Implementation

The model was applied to the Gulf of Thailand (about 400 km x 800 km). Grid size of 0.2 degree by 0.2 degree was chosen in order to optimize both accuracy and memory usage. The water column was divided into three layers, surface (0-10 m), mid-depth (10-40), and bottom (>40 m). The

bottom layer was generally represented deep-water below the pycnocline which was well developed in the Gulf of Thailand.

Because the data from the collaborative research alone did not cover the entire Gulf, we decided to supplement SEAFDEC data with long-term data available from WDC-A (Oceanography) and JODC for the same months. One these data were available, they enable us to perform additional simulations for other months so that the intra-annual trends among seasons can be seen.

Since the data for some months did not evenly cover the whole Gulf, we combined data into 4 groups according to the monsoon regimes, December-February (Northeast Monsoon), March-May (First Inter-Monsoon), June-August (Southwest Monsoon) and September-November (Second Inter-Monsoon). By this way the whole area of the Gulf was well blanketed by data points. The numbers of stations used in these four simulations are 1779, 858, 1145 and 1314, respectively.

The observed temperature and salinity data (both CTD and serial station data) within each of the three depth intervals were averaged. The spatial data of temperature, salinity and bottom depth were subsequently gridded using Krigging Method (Kegler, 1994). The gridded data was formatted according to the requirement of the model which was written in FORTRAN.

The condition and parameter used in each simulation are given in Tables 1 and 2.

Results and Discussion

Northeast Monsoon Season (December-February)

Surface temperature during the Northeast Monsoon (Fig. 1a) shows that the water from the Chao Phraya River systems had temperature that was 1-2 °C lower than surface temperature in the Gulf. Sea surface temperature was lower along the west than the east coast. There was also a plume of low salinity from Tapi River system that extended as far as 100 km from shore (Fig. 1b). Apparently there has been no explanation for this plume since the runoff from this river system in this season should not be more than 50 m³/s which was much less than that in the Upper Gulf of Thailand. Mid-depth temperature and salinity distribution were in general agreement to those at the surface (Figs. 2a and 2b).

A strong meander was formed in surface layer and the general direction of flow along the meander was toward the head of the Gulf (Fig. 1c). There was also a small counter clockwise eddy near the center of the Gulf.

Along the western half of the Gulf, surface current was westward toward the coast of the peninsular (Fig. 1c). However the mid-depth water flowed in an opposite direction (Fig. 2c). The water balance indicated a net gain of water in the Gulf and that was well supported by observations by the others that sea level in the Gulf was higher during the Northeast Monsoon.

Deep water temperature and salinity below the pycnocline (Figs. 3a and 3b) clearly suggested an intrusion of intermediate water from the South China Sea along the shore of Vietnam and Cambodia. Deep water circulated anticlockwisely and exited the Gulf along the west coast. The speed of the deep water current was less than 5 cm/s (Fig. 3c).

First Inter-Monsoon Season (March-May)

According to the temperature and salinity, surface and mid-depth waters in the Gulf in this season was well distinguished from the South China Sea water (Figs. 4a, 4b, 5a and 5b). A weak counterclockwise eddy was formed near the mouth of the Gulf and a clockwise eddy was formed in Cambodian EEZ (Figs. 4c and 5c). In general the direction of surface flow in the lower part of the Gulf, Songkhla and below, was outward. However, to the north of Songkhla, surface water along the west coast flew northward. Surface current speed was apparently slow (mostly less than 10 cm/s) relative to surface velocity in other seasons.

There was a prominent tongue of low temperature high salinity water extended from the South

China Sea into the central deep basin of the Gulf (Figs. 6a and 6b). The velocity of this inward flow of deep water was quite strong (up to 10 cm/s, Fig. 6c) compare to the deep water velocity during the Northeast Monsoon.

Southwest Monsoon Season (June-August)

Sea surface and mid-depth temperature of the Gulf were higher near the center of the Gulf and spread along the southwest coast, toward the Thai-Malaysian border (Figs. 7a and 8a). Surface and mid-depth salinity indicated that the head of the Upper Gulf and all the east coast of the Gulf from Thailand through Cambodia to Vietnam were major sources of freshwater input (Figs. 7b and 8b). These near surface plumes of low salinity water along the east coast however were unlikely to cross the southeastward meander which was well developed roughly along the central axis of the Gulf. The velocity along this meander was up to 40 cm/s but there was no eddy formed in the surface layer in this simulation (Fig. 7c). Nevertheless the low salinity water from the eastern side of the gulf could cross the central axis of the Gulf at the mid-depth layer where the meander was much weaker. A mid-depth clockwise eddy was also evident in the northern part of the Gulf confirming the difference in the circulation characteristics between surface and mid-depth layers. The general flow pattern in the mid-depth layer near the mouth was southwestward, i.e. from the Cambodia-Vietnam EEZ to the Thai-Malay Peninsular (Fig. 8c).

Inflow of intermediate water from the South China Sea into the sub-pycnocline layer of the Gulf was extended as far north as 10°N (Figs. 9a and 9b). The velocity was also quite strong (up to 10 m/s, Fig. 9c) but considerably less than the velocity found in the First Inter-Monsoon Period.

Second Inter-Monsoon Season (September-November)

Plume of Upper Gulf water characterized by its relatively higher temperature was well observed in the surface and mid-depth layers as far south as the center of the Gulf. This southward plume might had been merging with another high temperature water from Nakorn Sri Thamarat (Figs. 10a and 11a). The water originated from Cambodia easily distinguished by its low salinity was confined only to the southeastern portion of the Gulf near the mouth and did not cross the central axis toward the Thai-Malay Peninsular (Figs. 10b and 11b). The surface current vectors were southeastward into the South China Sea (Fig. 10c) while the mid-depth current vectors were mostly eastward with a small counterclockwise eddy near the center of the Gulf (Fig. 11c) indicating replenishment of surface water by mid-depth water.

Deep water in this season in the Gulf in terms of temperature and salinity was indistinguishable from intermediate water of the South China Sea (Figs. 12a and 12b). The northwestward inflow of South China Sea water, although could be seen (Fig. 12c), the magnitude was less than that in the previous season which might indicate an intermediate stage of changing of the monsoonal effect. No clear eddies or meanders were seen in this simulation.

Table 1. Assumptions and constants used for all runs

Constants	Value
Grid size	0.2 x 0.2 degree (2.22 x 10 ⁶ cm ²)
Surface layer	0-10 m
Mid-depth layer	10-40 m
Bottom layer	>40 m
Lateral boundary drag	Full slip
Gravity wave	None
Bottom drag coefficient	0.0026
Median latitude	9° N
Tidal forcing at boundaries	None
(Open) Boundary values	
· Surface temperature	30 °C
· Mid-depth temperature	28 °C
· Bottom temperature	28 °C
· Surface salinity	33 psu
· Mid-depth salinity	33 psu
· Bottom salinity	33 psu
Surface wind drag coefficient	0.0013
Solar heating	
· Mean	5.72 x 10 ⁻³ cal cm ⁻² s ⁻¹
· Amplitude variation	5.73 x 10 ⁻⁴ cal cm ⁻² s ⁻¹
· Phase	0
· Frequency	2.02 x 10 ⁻⁷ s ⁻¹
River discharge	None
Run time	10 days
Time step	240 s
Eddy viscosity	
· Horizontal	1.0 x 10 ⁷ cm s ⁻¹
· Vertical	3.0 x 10 ⁷ cm s ⁻¹
Eddy diffusivity	
· Horizontal	5.0 x 10 ⁷ cm s ⁻¹
· Vertical	5.0 cm s ⁻¹

Table 2. Variables for each run

	Dec.-Feb.	Mar.-May	Jun.-Aug.	Sep.-Nov.
Wind (m/s)	5 (NE)	2 (SE)	5 (SW)	5 (SW)
Temperature	Tri-monthly averaged of SEAFDEC, NODC and JODC data			
Salinity	Tri-monthly averaged of SEAFDEC, NODC and JODC data			

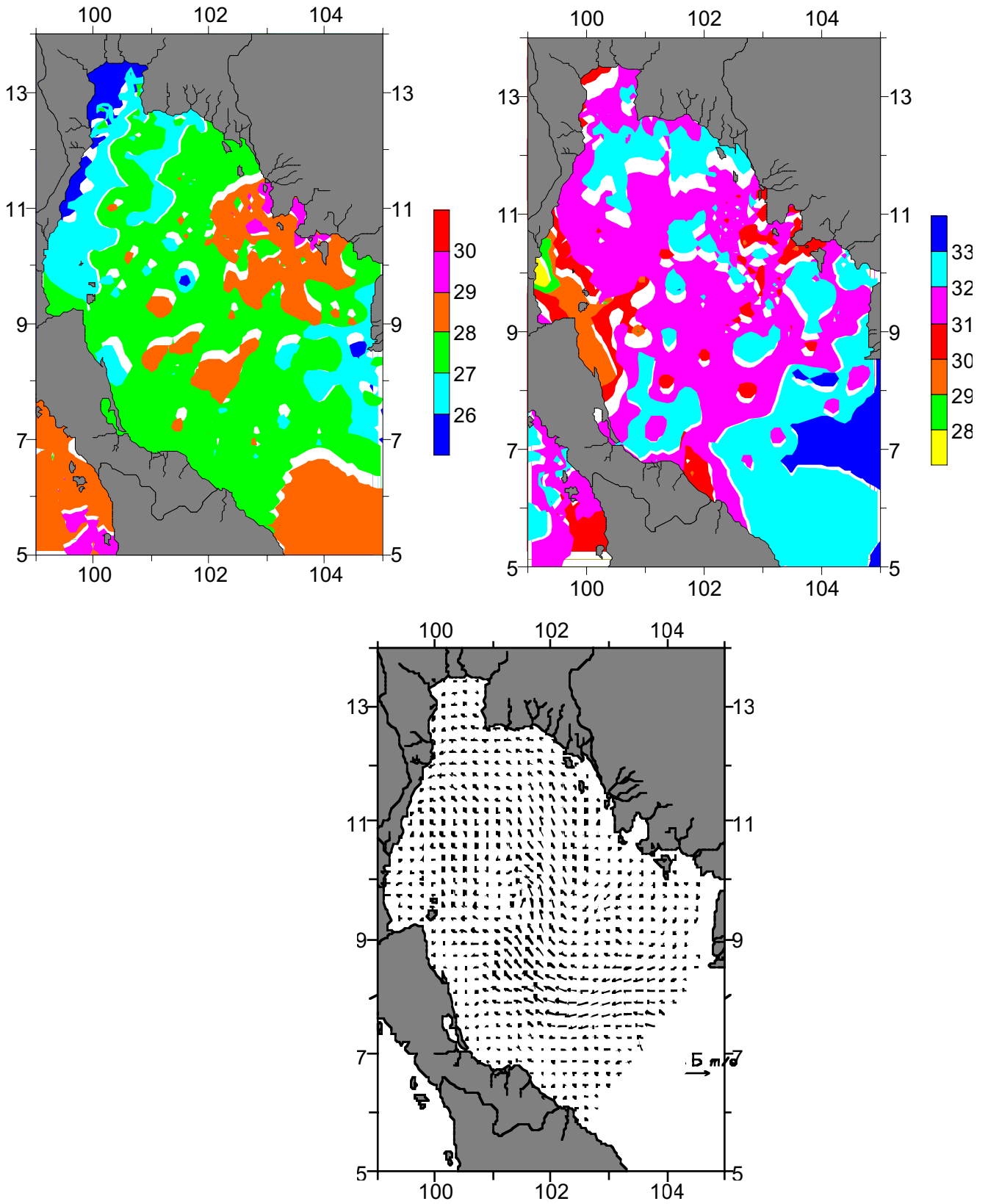


Fig. 1. December-February surface (0-10 m) contours of (a) temperature and (b) salinity, and (c) current vector field. Observation points are given as +.

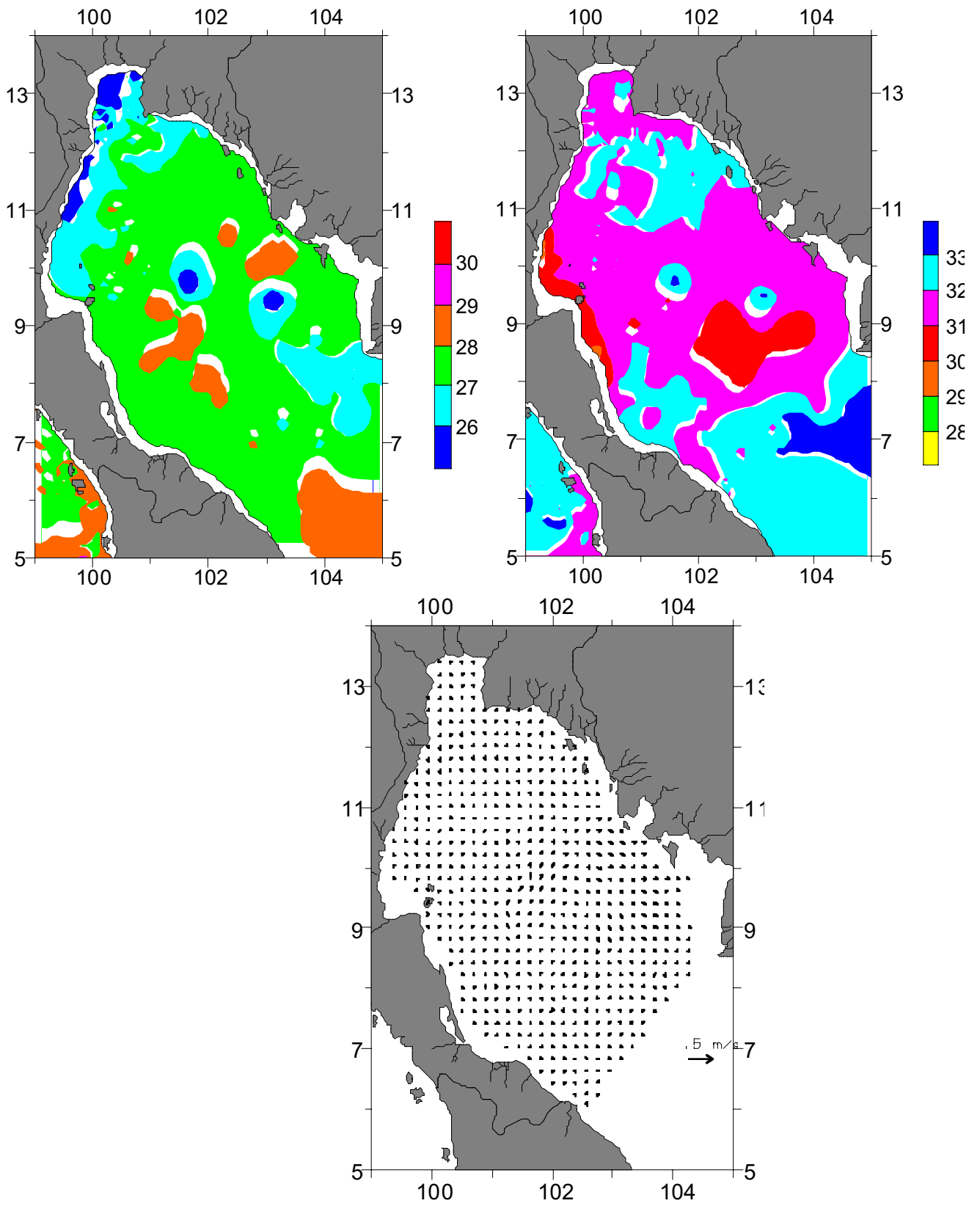


Fig. 2. December-February mid-depth (10-40 m) contours of (a) temperature and (b) salinity, and (c) current vector field. Observation points are given as +.

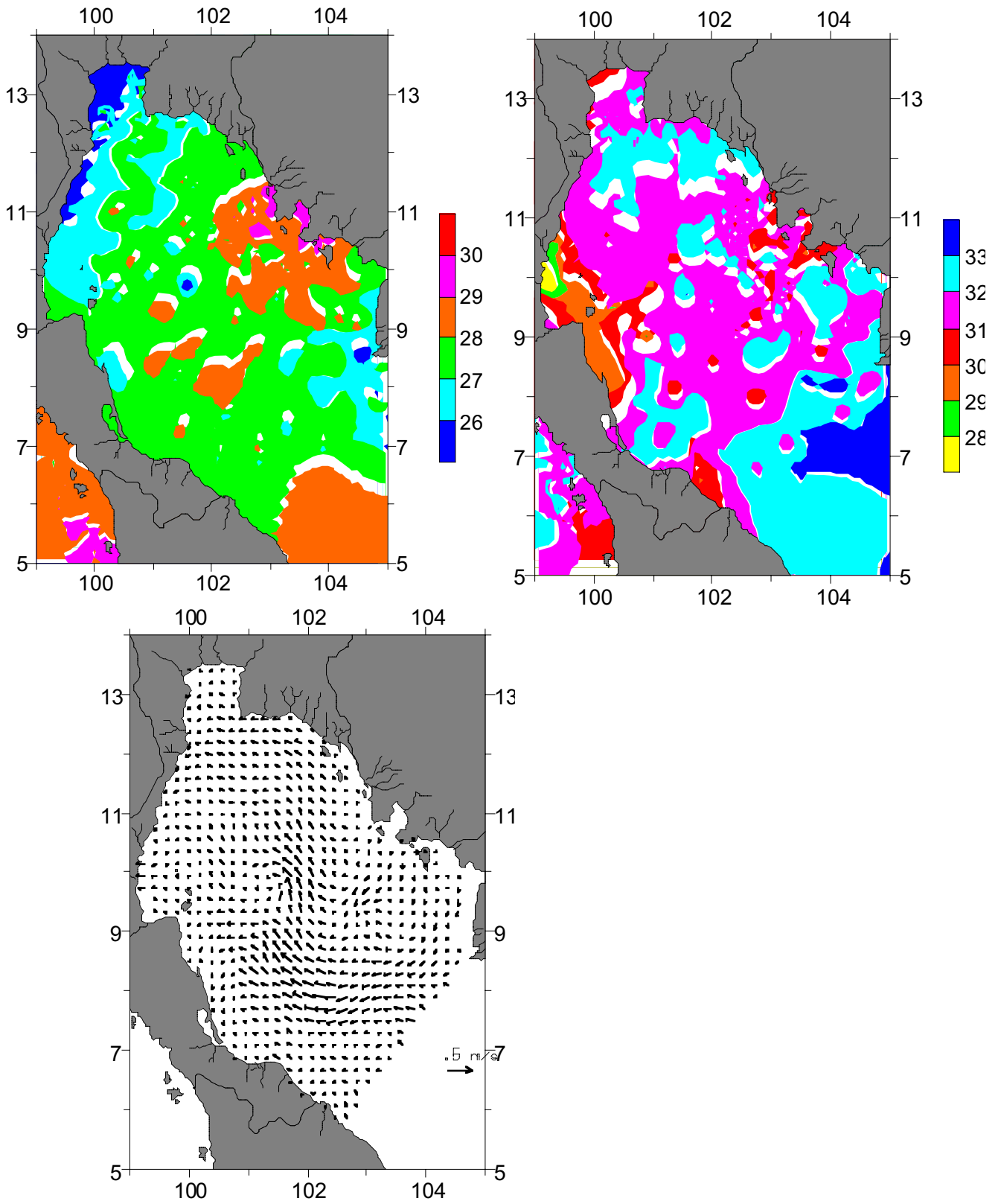


Fig. 3. December-February deep-water (>40 m) contours of (a) temperature and (b) salinity, and (c) current vector field. Observation points are given as +.

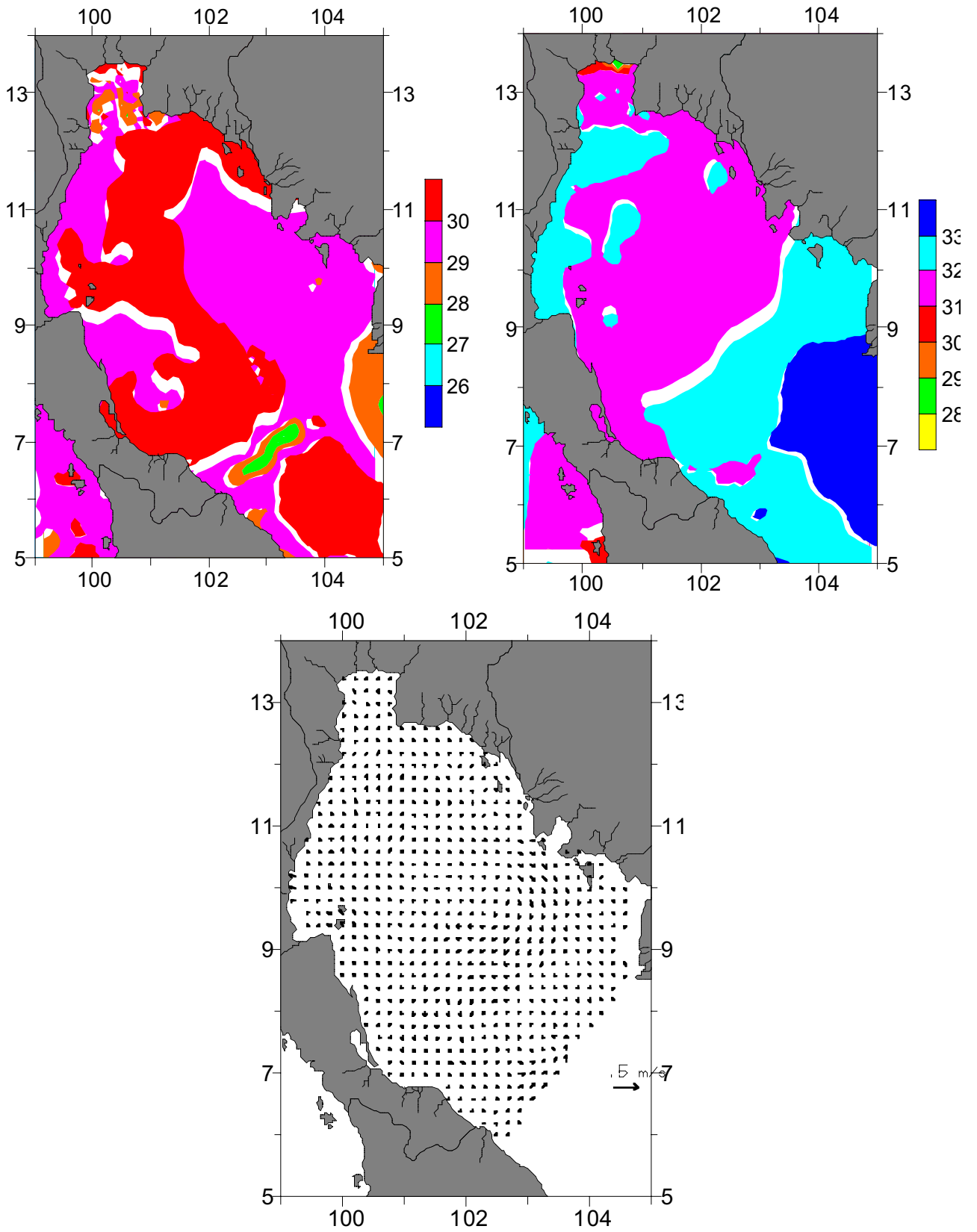


Fig. 4. March-May surface (0-10 m) contours of (a) temperature and (b) salinity, and (c) current vector field. Observation points are given as +.

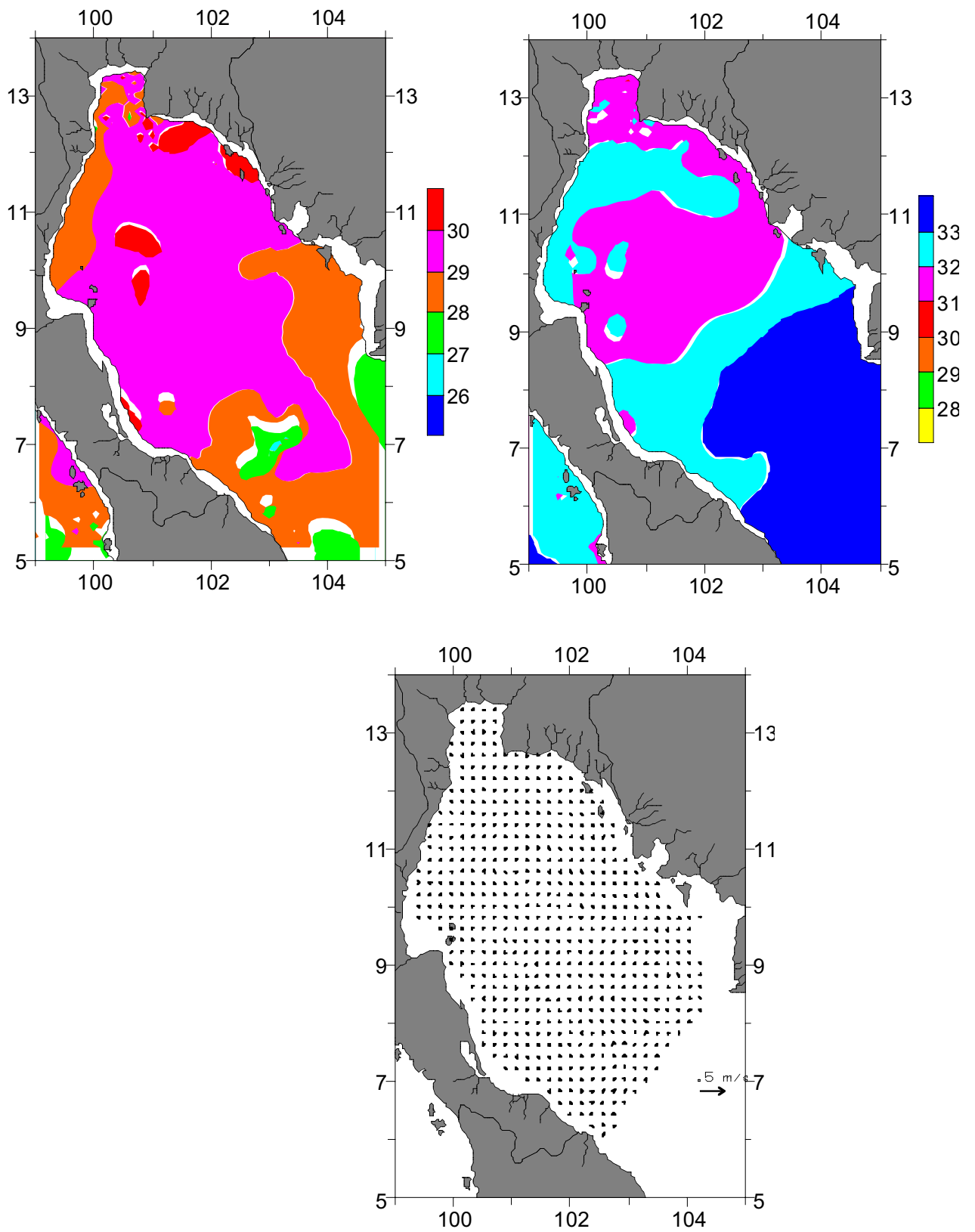


Fig. 5. March-May mid-depth (10-40 m) contours of (a) temperature and (b) salinity, and (c) current vector field. Observation points are given as +.

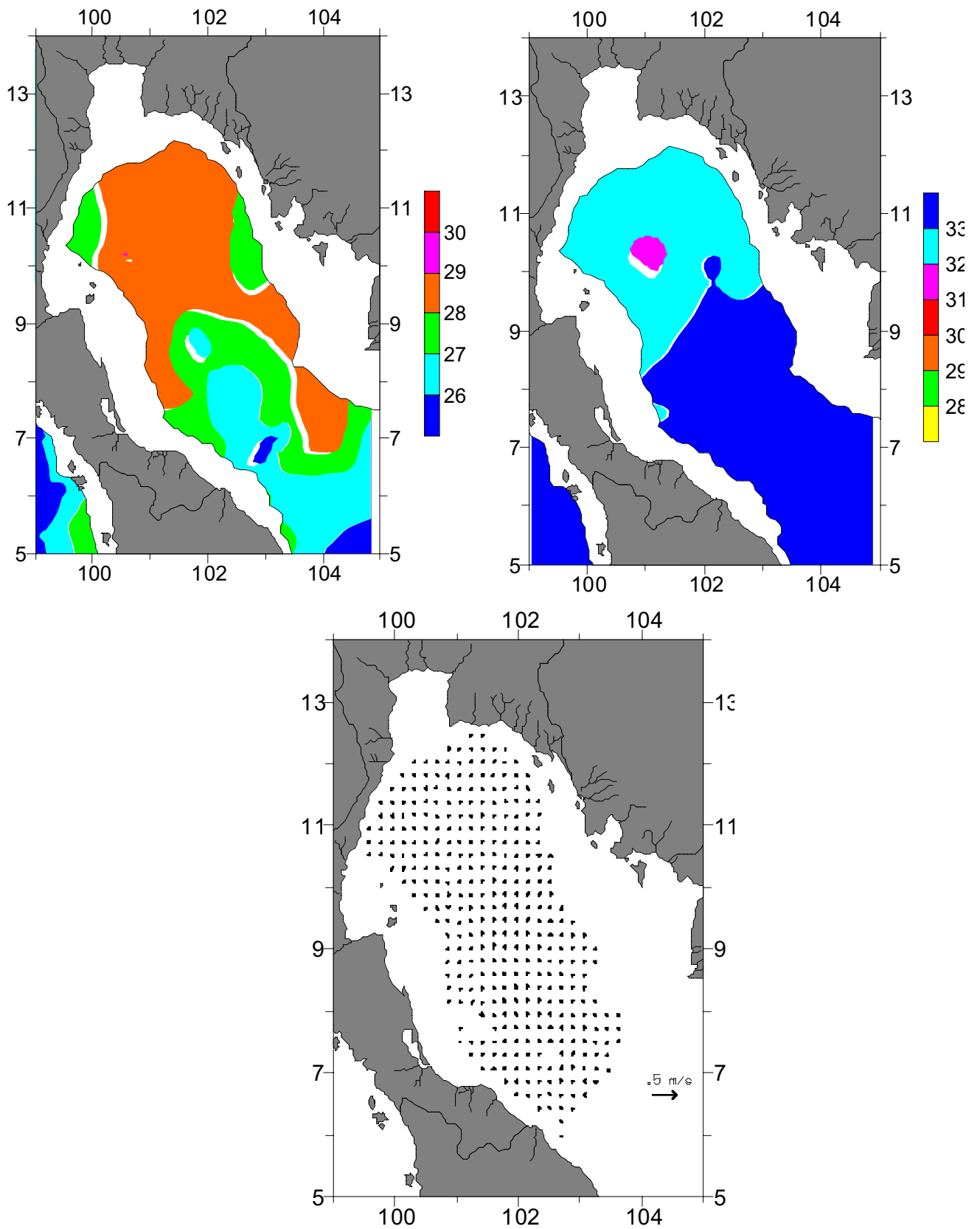


Fig. 6. March-May deep-water (>40 m) contours of (a) temperature and (b) salinity, and (c) current vector field. Observation points are given as +.

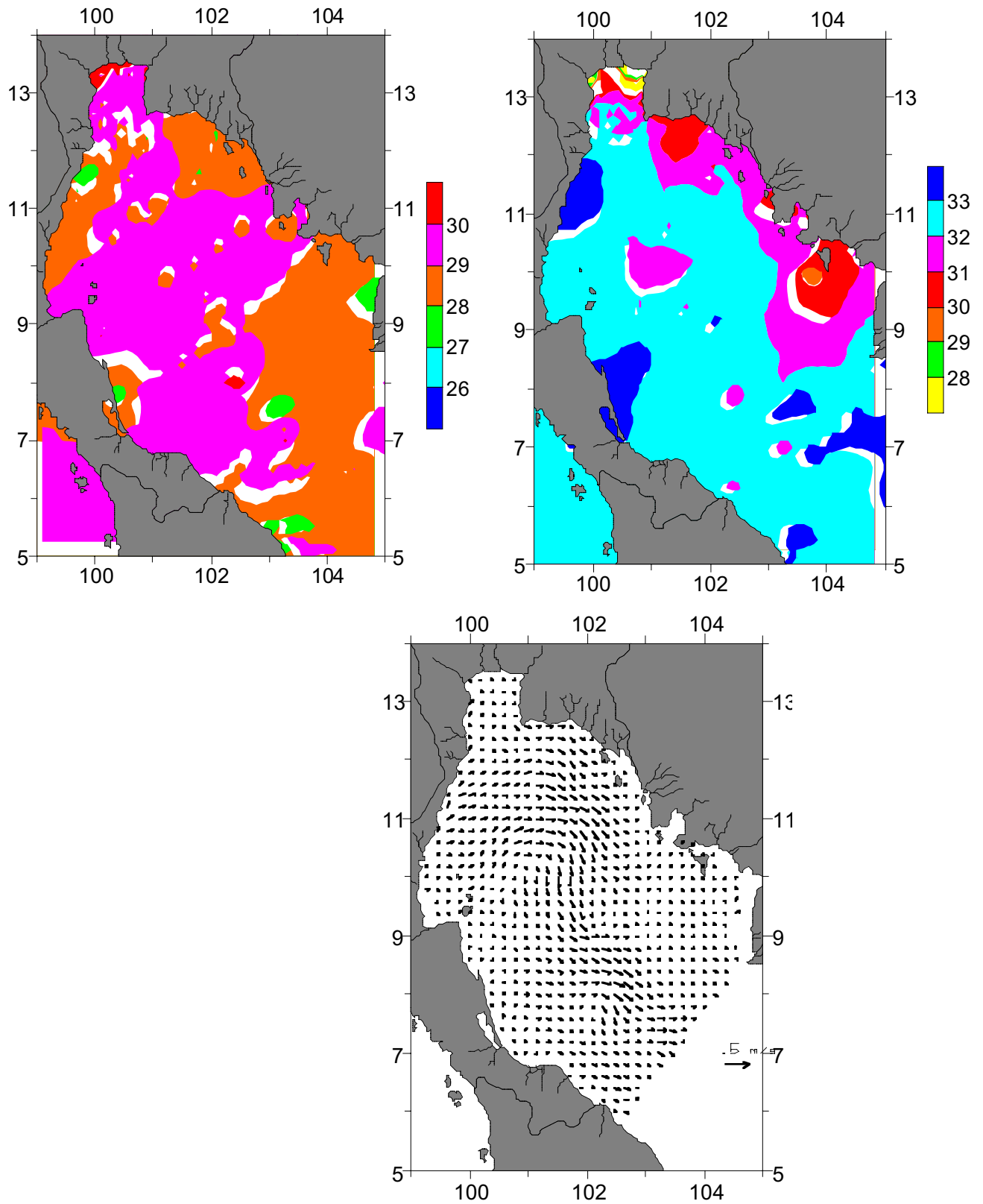


Fig. 7. June-August surface (0-10 m) contours of (a) temperature and (b) salinity, and (c) current vector field. Observation points are given as +.

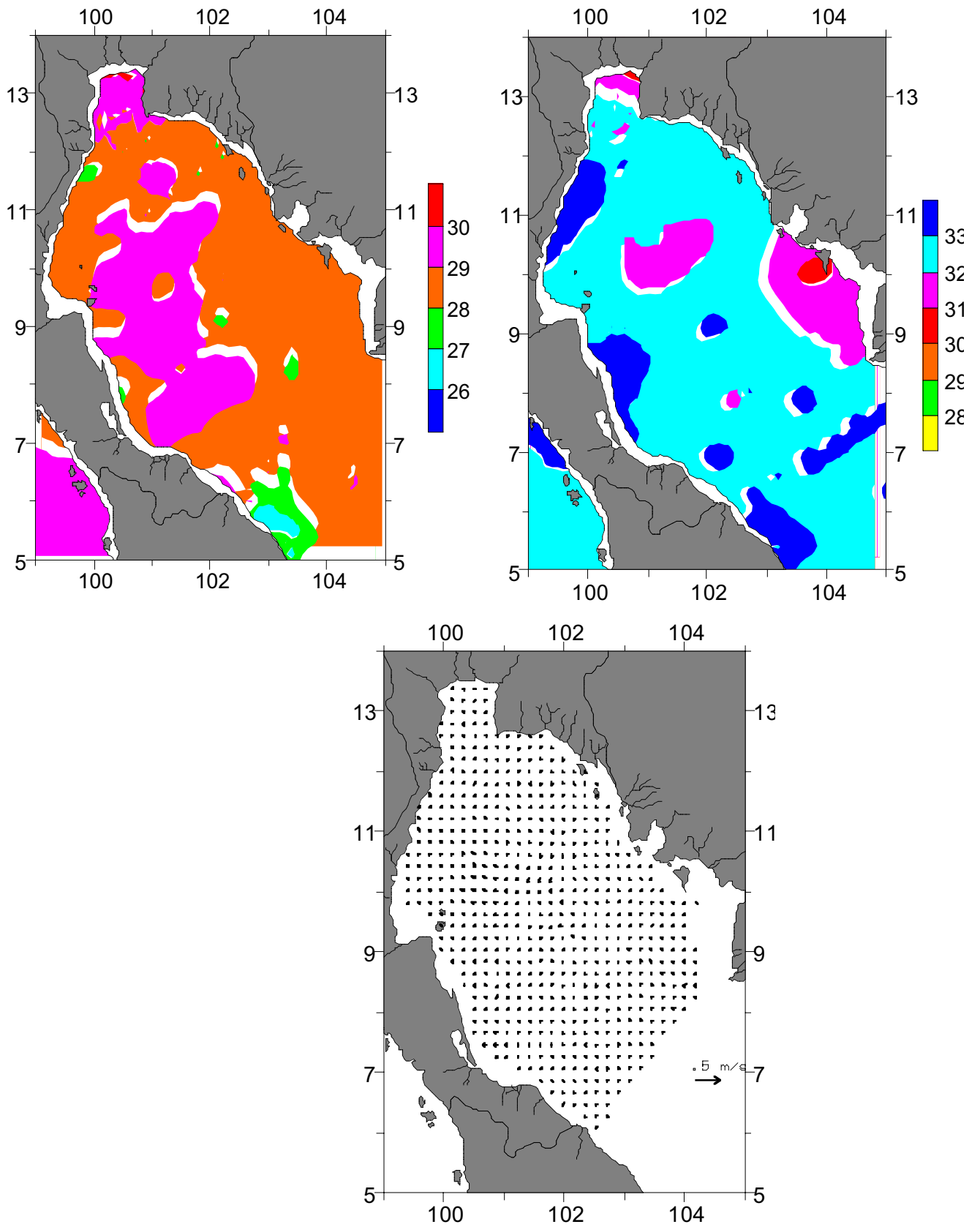


Fig. 8. June-August mid-depth (10-40 m) contours of (a) temperature and (b) salinity, and (c) current vector field. Observation points are given as +.

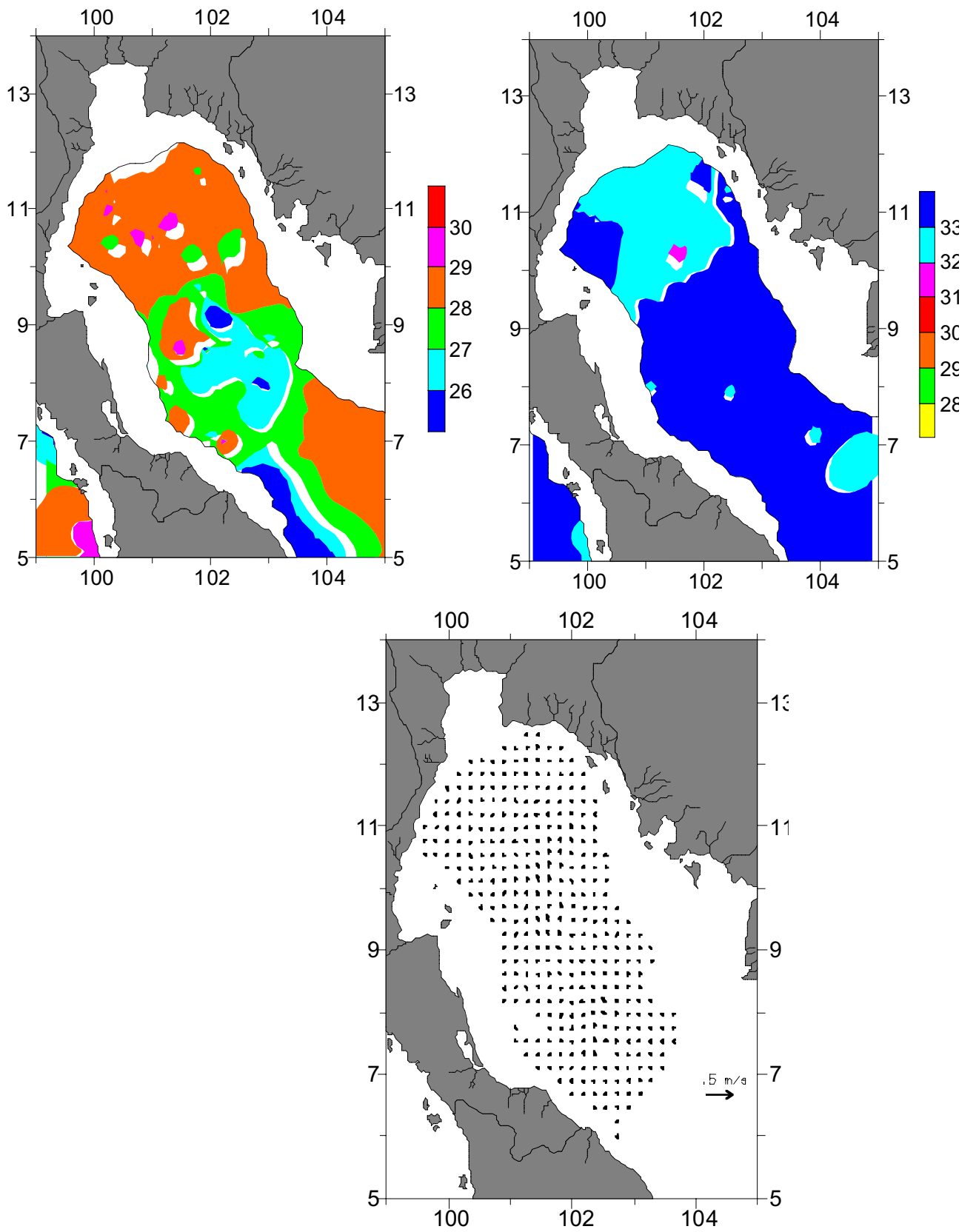


Fig. 9. June-August deep-water (>40 m) contours of (a) temperature and (b) salinity, and (c) current vector field. Observation points are given as +.

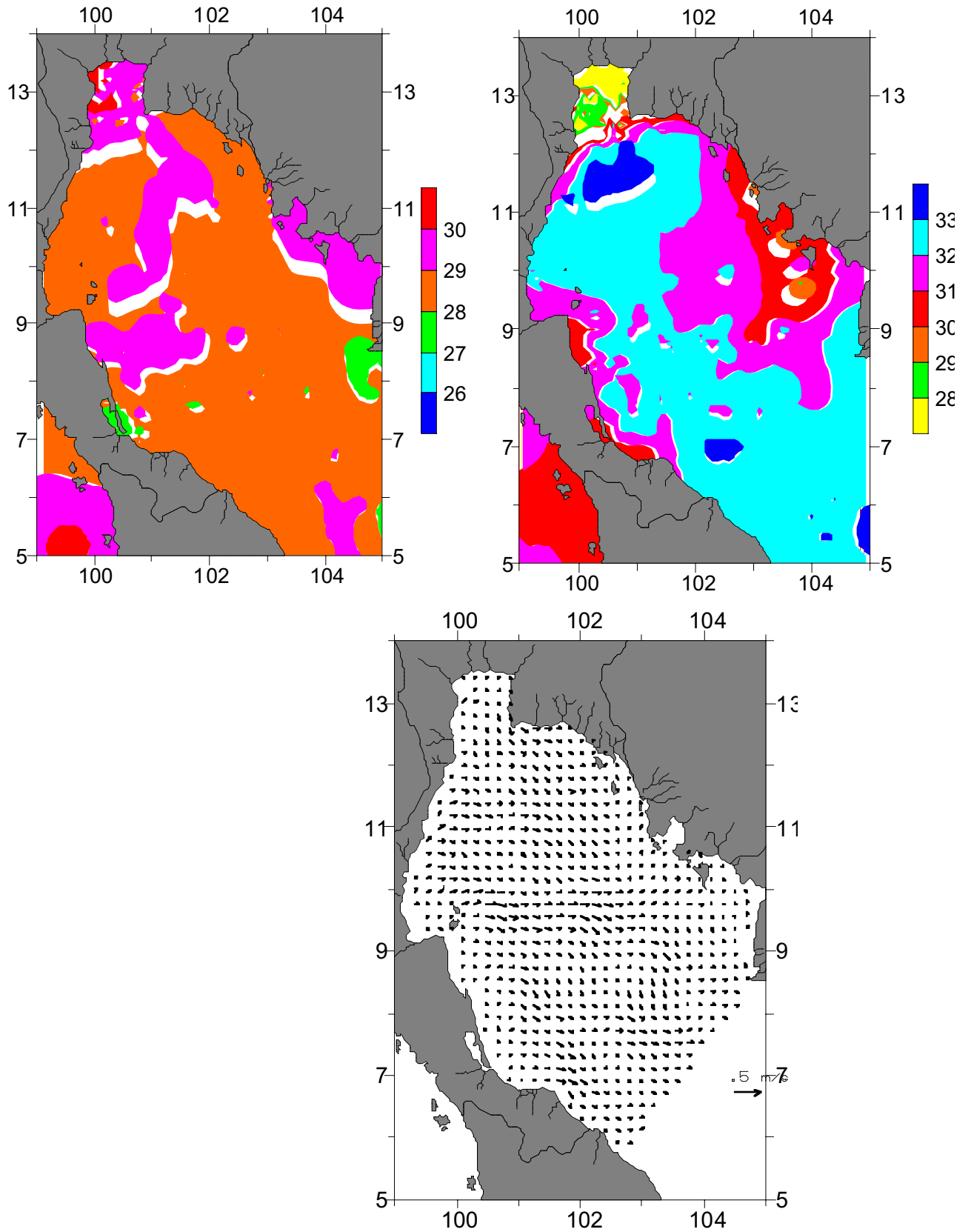


Fig. 10. September-November surface (0-10 m) contours of (a) temperature and (b) salinity, and (c) current vector field. Observation points are given as +.

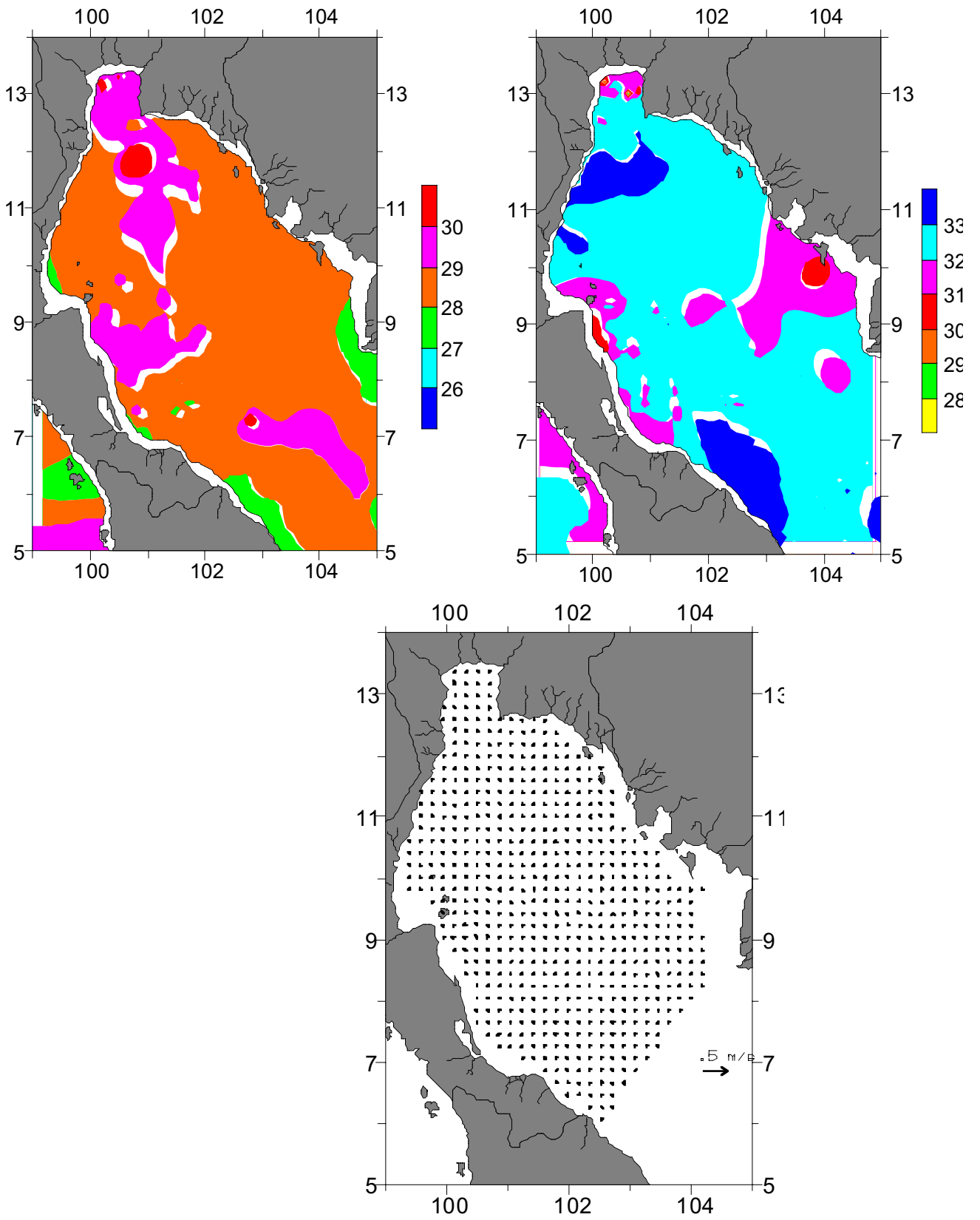


Fig. 11. September-November mid-depth (10-40 m) contours of (a) temperature and (b) salinity, and (c) current vector field. Observation points are given as +.

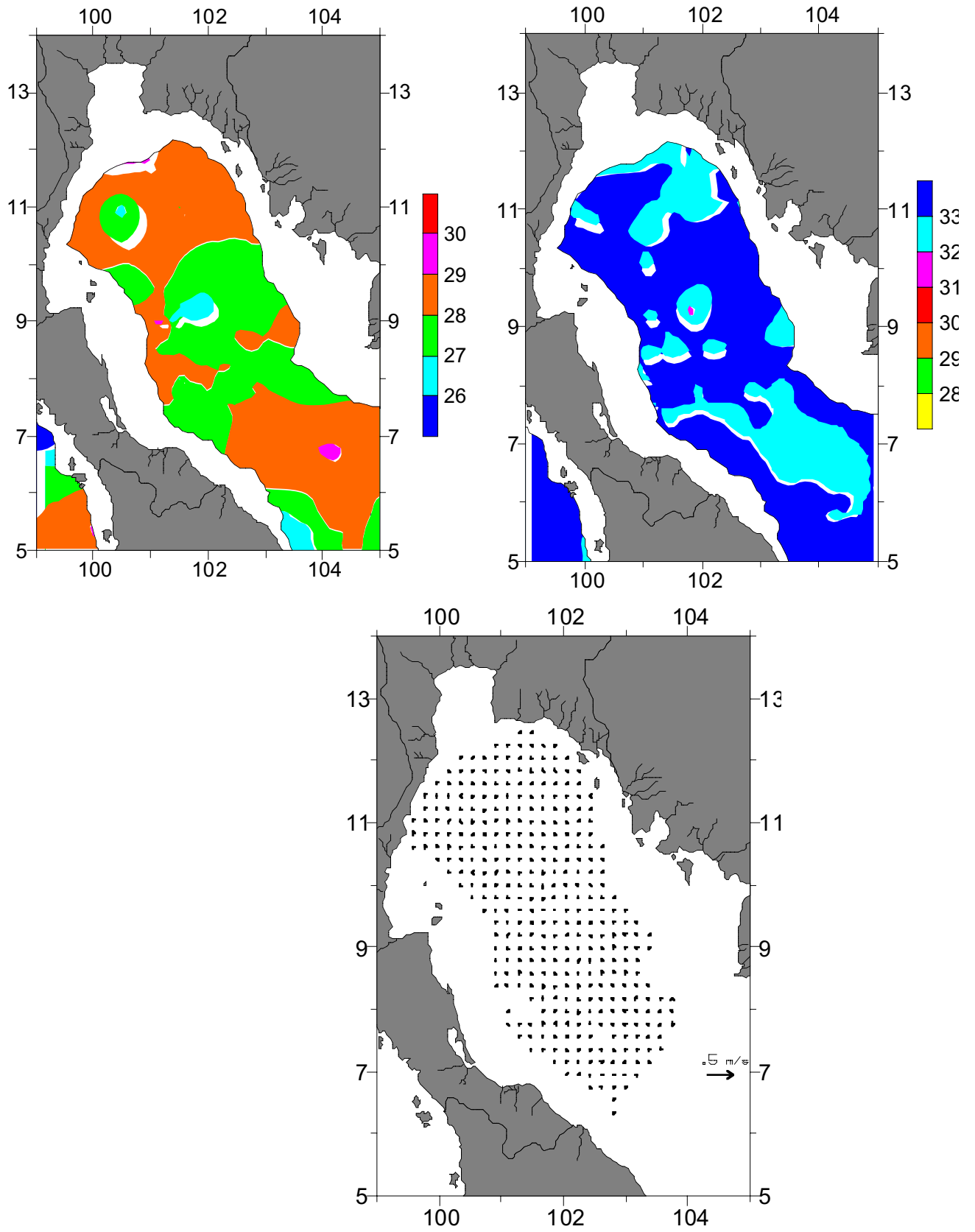


Fig. 12. September-November deep-water (>40 m) contours of (a) temperature and (b) salinity, and (c) current vector field. Observation points are given as +.

Conclusion and Recommendations

- 1) Surface current (0-10 m) in the Gulf of Thailand was strongly influenced by prevailing Monsoon. The surface vector field was northeastward in to the Gulf from the South China Sea during the Northeast Monsoon and opposite during the Southwest Monsoon.
- 2) Mid-depth (10-40 m) flow was more or less in opposite to the surface current in every season which suggested that the major replenishment of water in the surface layer was by the mid-depth layer. Because the water from these two layer had generally the same chemistry, this vertical replenishment of surface water would not supplement surface water by nutrient enrichment.
- 3) Water flow in the central deep basin (>40 m) also changed direction among seasons. This might be due to density gradient rather than wind. It was not clear from the simulations that whether this nutrient enriched deep water was actually “upwelled” to the surface.
- 4) Contrary to some previous believes, the simulations in this study did not reveal any true circulation gyres in the Gulf. However, eddies and meanders of different degrees could be developed. These physical features could play very important role in the distribution and dispersion of chemicals, particles and biological species.
- 5) More detailed simulations must be done in order to get a more realistic picture of circulation in the Gulf, including fine scale characteristics.

References

- Backhaus, J. O. 1983. A semi-implicit scheme for the shallow water equation for application to shelf water sea modeling. *Continental Shelf Res.* 2: 243-254.
- Fujio, S. and Imasato, N. 1991. Diagnostic calculation and water mass movement in the deep Pacific. *J. Geophys. Res.* 96: 759-774.
- Kegler, 1994
- Roed, L. P. and Cooper, C. K. 1986. Open boundary conditions in numerical ocean models. In: *Advance Physical Oceanographic Numerical Modeling*. J. J. O'Brien (ed.). Kluwer Academic Publishers, Massachusetts, pp. 411-433.
- Sarmiento, J. L. and Bryan, K. 1982. An ocean transport model for the North Atlantic. *J. Geophys. Res.* 87: 394-408.
- Sojisuporn, P. 1995. Density-driven and Wind-driven Current in The Upper Gulf of Thailand. Research report submitted to the National Research Council of Thailand, 23 pp.
- Yanagi, T. and Takahashi, S. 1993. Seasonal variation of circulations in the East China Sea and the Yellow Sea. *J. Oceanogr.* 49: 503-520.